Published in final edited form as:

Biosci Rep. 2011 April ; 31(2): 151–158. doi:10.1042/BSR20100110.

Snapin deficiency is associated with developmental defects of the central nervous system

Bing ZHOU[*,†,1], **Yi-Bing ZHU**[*,†,1], **Lin LIN**[†,1], **Qian CAI**[*], and **Zu-Hang SHENG**[*,2]

[*]Synaptic Function Section, National Institute of Neurological Disorders and Stroke, National Institutes of Health, 35 Convent Drive, Bethesda, MD 20892-3706, U.S.A

[†]Department of Neurobiology, Shanghai Jiao-Tong University School of Medicine, Shanghai, People's Republic of China

Synopsis

The autophagy–lysosomal pathway is an intracellular degradation process essential for maintaining neuronal homoeostasis. Defects in this pathway have been directly linked to a growing number of neurodegenerative disorders. We recently revealed that Snapin plays a critical role in co-ordinating dynein-driven retrograde transport and late endosomal–lysosomal trafficking, thus maintaining efficient autophagy–lysosomal function. Deleting *snapin* in neurons impairs lysosomal proteolysis and reduces the clearance of autolysosomes. The role of the autophagy–lysosomal system in neuronal development is, however, largely uncharacterized. Here, we report that *snapin* deficiency leads to developmental defects in the central nervous system. Embryonic *snapin*$^{-/-}$ mouse brain showed reduced cortical plates and intermediate zone cell density, increased apoptotic death in the cortex and third ventricle, enhanced membrane-bound LC3-II staining associated with autophagic vacuoles and an accumulation of polyubiquitinated proteins in the cortex and hippocampus. Thus our results provide *in vivo* evidence for the essential role of late endocytic transport and autophagy–lysosomal function in maintaining neuronal survival and development of the mammalian central nervous system. In addition, our study supports the existence of a functional interplay between the autophagy–lysosome and ubiquitin–proteasome systems in the protein quality-control process.

Keywords

apoptotic cell death; autophagy; late endocytic trafficking; lysosome; neuronal development; ubiquitin

[2]To whom correspondence should be addressed (shengz@ninds.nih.gov).
[1]These authors contributed equally to this work.

AUTHOR CONTRIBUTION

Bing Zhou, Yi-Bing Zhu and Lin Lin conducted the experiments and analysed the data; Qian Cai helped design the experiments: and Zu-Hang Sheng is the senior author responsible for the project design and writing the manuscript.

INTRODUCTION

Neuron maintenance and survival require retrograde transport of late endocytic organelles from synaptic terminals and distal processes to the soma, where late endocytic trafficking events deliver target materials and internalized proteins to lysosomes for degradation [1]. Autophagy is a homoeostatic process whereby autophagosomes deliver bulk cytoplasmic components and organelles to lysosomes by forming degradative autolysosomes. These two processes rely on the same late endocytic trafficking pathway, which is crucial for the maturation and degradative capacity of the autophagy–lysosomal system.

Dynein-driven retrograde transport of late endocytic organelles is particularly challenging for neurons, as most acidic mature lysosomes are generated in the soma and proximal axon [2]. Thus elucidating the mechanisms regulating late endocytic transport and autophagy–lysosomal function in neurons will be critical for the understanding of clearance of aggregate-prone intracytosolic proteins that are associated with a range of neurodegenerative diseases. A recent study from our laboratory uncovered a new mechanism that regulates the autophagy–lysosomal function by co-ordinating two dynamic cellular processes: dynein-mediated late endocytic transport and endosome–lysosome trafficking [3]. Snapin acts as an adaptor that links late endosomes to the dynein motor through direct binding to dynein intermediate chain. Snapin–dynein-mediated retrograde transport is essential for the delivery of late endosomal cargo from distal processes to the soma, where late endosomes and lysosomes come into sufficient proximity for high-efficiency membrane trafficking by the motor-driven force. Such a mechanism enables neurons to maintain proper degradative capacity and cellular homoeostasis via the autophagy–lysosomal pathway.

An impaired autophagy–lysosomal system has been associated with the pathogenesis of neurodegenerative diseases [4,5]. Protein quality control via the autophagy–lysosomal system helps maintain cellular homoeostasis and therefore cell survival [6]. Mouse mutations in autophagy essential and regulatory elements result in early embryonic death [7] or embryonic survival but with nutrient and energy insufficiency soon after birth [8,9] and neurodegeneration [10,11]. In mouse embryos, functional deficiency of Ambra1, a positive regulator of autophagy, leads to severe neural tube defects associated with the accumulation of ubiquitinated proteins and increased apoptotic cell death [12]. How the processes linking late endocytic transport and the autophagy–lysosomal function regulate the development of the central nervous system is, however, largely uncharacterized.

Because *snapin*-KO (knockout) mice exhibit embryonic and neonatal death, in the present study, we investigated whether *snapin* deficiency in mice leads to developmental defects in the central nervous system. Our present study shows that *snapin*$^{-/-}$ embryonic mouse brains display reduced cell density, increased apoptotic death, enhanced LC3-II-labelled autophagic vacuoles and an aberrant accumulation of polyubiquitinated proteins. Thus the *snapin*−KO embryos provide us with a genetic tool for characterizing the role of late endocytic transport and the autophagy–lysosomal system in embryonic development of the mammalian central nervous system.

MATERIALS AND METHODS

Animal handling

The care and use of animals were carried out in accordance with NIH (National Institutes of Health) guidelines and were approved by the Animal Care and Use Committee of the National Institute of Neurological Disorders and Stroke/National Institute on Deafness and Other Communication Disorders, NIH.

Immunocytochemistry

E18 (embryonic day 18) *snapin*$^{+/+}$ and *snapin*$^{-/-}$ mouse pups were removed from the uterus and dissected in ice-cold Hanks balanced salt solution. The brain was removed and fixed in 4% (w/v) paraformaldehyde in PBS. The whole brain was embedded in paraffin and sectioned into 8 μm-thick slices. Three animals were used for each genotype. For the cell density study, 15 coronal sections were chosen from each animal. Cells were stained with haematoxylin and eosin (Fisher Scientific). NIH ImageJ was used to quantify cell density. Antibodies specific for the neuronal nuclear marker NeuN (neuronal nuclei) (Chemicon) and ubiquitin (Dako) were used as per the manufacturer's instructions, followed by TO-PRO-3 (Invitrogen) staining.

The Apotag Plus Peroxidase In Situ kit (Chemicon) was used for TUNEL (terminal deoxynucleotidyl transferase-mediated dUTP nick-end labelling) staining. Briefly, the paraffin-embedded tissue was washed three times with xylenes, followed by three washes with ethanol. After treating with freshly prepared Protein K (20 μg/ml), TdT (terminal deoxynucleotidyl transferase) and digoxigenin conjugate were applied directly to the samples to visualize the apoptotic cells. TUNEL-positive cells were counted at ×40 magnification (fields per brain slice) and expressed as a percentage ratio of the total cell number as determined by fluorescence.

For LC3 staining, the paraffin-embedded tissue slices were deparaffinized in xylene and retrieved by microwaving for 20 min in 0.01 M citrate buffer and subsequently cooled in retrieval buffer for 40 min. The slices were incubated with 20% (v/v) NGS (normal goat serum) plus 0.4% saponin at room temperature (25°C) for 30 min and probed with an anti-LC3 antibody (Novus Biologicals) at room temperature for 30 min. After three washes with 1× PBS, the fluorescent conjugate anti-IgG antibody (Molecular Probes) was used.

Image acquisition

Confocal images were obtained using a Zeiss LSM 510 microscope with sequential-acquisition settings. For fluorescence quantification, images were acquired below saturation using the same settings at 1024 × 1024 pixels resolution (12 bit). Morphometric measurements were made using Image-Pro Plus (Media Cybernetics), Metamorph (Universal Imaging) or NIH ImageJ.

Immunoblots

Brains from E18 *snapin*$^{+/+}$ and *snapin*$^{-/-}$ mice were homogenized in TBS buffer [50 mM Tris/HCl, pH 7.4, 150 mM NaCl, 1% Triton X-100, plus protease inhibitors (1 mM PMSF,

10 mg/ml leupeptin and 2 mg/ml aprotinin)]. A 20 μg portion of the homogenates was loaded, processed for SDS/PAGE and sequentially detected with monoclonal antibodies against ubiquitin (Santa Cruz Biotechnology) and p115 (BD Transduction Laboratories), and a polyclonal antibody against Snapin (SYSY). Horseradish-peroxidase-conjugated secondary antibodies and ECL® (enhanced chemiluminescence) reagents (GE Healthcare) were used to visualize proteins of interest. For detection with different antibodies, blots were stripped in a solution of 62.5 mM Tris/HCl (pH 7.5), 20 mM dithiothreitol and 1% SDS for 20 min at 50°C with agitation and subsequently subjected to two washes each for 15 min in TBS/0.1% Tween 20.

For quantitative analysis, protein bands detected by ECL® were scanned into Adobe Photoshop CS3 and analysed using Gel-Pro 4.5 protein imaging software (Media Cybernetics). During the exposure of the ECL® film, care was taken that intensity readouts were in the linear range of the standard curve blot detected with the same antibody. The normalized percentage of polyubiquitin and Snapin levels from *snapin*-deficient mice relative to that of WT (wild-type) littermates was calculated using standard curves for the same proteins. The results of Student's *t* tests for three pairs of *snapin* littermates are expressed as means ± S.E.M.

Statistical analysis

Images are representative of > 15 sections from three pairs of littermates. Immunoblots are representative of six experiments. Statistical analyses were performed using the Student's *t* test and are presented as means ± S.E.M.

RESULTS

Reduced cell density in cortical plates and intermediate zones of *snapin*$^{-/-}$ embryonic mouse brains

Snapin-KO mice generated from the inbred BL/6J line were recovered at an atypical proportion (0.24:0.58:0.18) due to increased lethality before E14.5 for homozygotes. Homozygous mutant pups are smaller than WT pups and die within 6 h of birth. There were no observable changes in mouse development between *snapin* heterozygous (*snapin*$^{+/-}$) and WT (*snapin*$^{+/+}$) littermates. Our previous study showed that *snapin* deficiency results in defective priming of large dense-core vesicles for fusion in mouse chromaffin cells [13] and reduced and unsynchronized synaptic vesicle release in mouse cortical neurons [14]. Impaired synaptic transmission, however, is not sufficient to explain why the homozygous deletion of *snapin* causes mouse perinatal death.

In addition to its association with synaptic vesicles, Snapin is present in membrane-associated fractions [15], is co-purified with BLOC-1 (biogenesis of lysosome-related organelle complex-1) [16] and is enriched in the late endocytic membrane [17], highlighting its multivalent role in intracellular trafficking events. Using biochemical, cellular and time-lapse imaging approaches in *snapin* mutant cortical neurons, combined with gene rescue experiments, we recently revealed that Snapin plays a critical role in co-ordinating late

endocytic transport and lysosomal maturation, two dynamic cellular processes required for the proper function of the neuronal autophagy–lysosomal system [3].

To determine whether *snapin* deficiency also affects embryonic central nervous system development, we co-stained paraffin sections from *snapin*$^{+/+}$ and *snapin*$^{-/-}$ brains at E18 with haematoxylin and eosin. The cerebral cortex and hippocampus in *snapin*$^{-/-}$ embryos are smaller than those of WT littermates (Figure 1A). These alterations are most prominent in the cortical plates and intermediate zones of *snapin*$^{-/-}$ mice compared with their *snapin*$^{+/+}$ littermates. The normalized cell densities in the cortical plates are 100 ± 1.31 for *snapin*$^{+/+}$ and 77.09 ± 2.49 for *snapin*$^{-/-}$ ($P < 0.001$, $n = 15$) and in the intermediate zones 100 ± 1.90 for *snapin*$^{+/+}$ and 76.02 ± 2.77 for *snapin*$^{-/-}$ ($P < 0.001$, $n = 15$). Consistently, the cell density was lower in the rostral level of *snapin*$^{-/-}$ embryonic brains (Figures 1B and 1C). Normalized cell densities in the rostral level of the cortical plates are 100.00 ± 1.60 for *snapin*$^{+/+}$ and 75.38 ± 1.87 for *snapin*$^{-/-}$ ($P < 0.001$, two-tailed Student's *t* test, $n = 15$) and in the intermediate zones 100.00 ± 2.51 for *snapin*$^{+/+}$ and 64.93 ± 2.23 for *snapin*$^{-/-}$ ($P < 0.001$, n=15). These results indicate that Snapin is critical for embryonic development of the central nervous system.

Increased cell death in the cortex and third ventricular region of *snapin*$^{-/-}$ embryos

Snapin deficiency results in reduced viability, axonal swelling and neurodegeneration in cultured neurons [3]. We next performed apoptosis analysis to determine whether the reduced neuron number observed in the *snapin*$^{-/-}$ embryonic brain was attributable to cell death. The TUNEL assay revealed a remarkable increase in cell death in the cerebral cortex and third ventricular region of E18 *snapin* mutant embryos (Figure 2A). Quantification analysis shows a significant increase in the average number of TUNEL-positive cells per field section of the cerebral cortex in *snapin*$^{-/-}$ embryos (4.69 ± 0.55, $n = 29$, $P < 0.001$) relative to *snapin*$^{+/+}$ brain (0.88 ± 0.15, n=41) (Figure 2B). The apoptotic cells in the third ventricular region of *snapin*$^{-/-}$ embryos are also significantly increased (19.03 ± 2.89, n=29, $P < 0.001$) compared with *snapin*$^{+/+}$ littermates (3.00 ± 0.53, $n = 31$). Thus, the reduction in neuron density observed in *snapin*$^{-/-}$ embryonic brains may be attributable, at least in part, to increased apoptosis.

Increased LC3-II-labelled autophagosomes in *snapin*$^{-/-}$ embryonic cortex

Snapin deficiency results in reduced maturation of lysosomes and impaired turnover of autolysosomes in cultured cortical neurons [3]. Reintroducing the *snapin* transgene into *snapin*$^{-/-}$ cells rescued the phenotype, indicating its critical role in maintaining a balance between the rate of autophagic sequestration and completion of degradation. To determine whether *snapin* deficiency impairs autophagy in the mouse embryonic central nervous system, we immunostained theE18 mouse cortex with an antibody against the autophagic marker LC3. This antibody detects two forms of LC3: cytosolic LC3-I and autophagic membrane-targeted LC3-II. LC3-II is a lipidated form of LC3-I and is eventually degraded by lysosomal hydrolases [18]. *Snapin* deletion in cultured cortical neurons increases the conversion of LC3 from cytosol into autophagic vacuoles, reflecting a reduced clearance of autolysosomes due to impaired lysosomal degradative capacity [3]. LC3 staining was primarily cytosolic and diffuse in the *snapin*$^{+/+}$ cortex (Figure 3A). In contrast, in *snapin*$^{-/-}$

mice, LC3-staining exhibits a vesicular punctate pattern throughout the cortex (Figure 3B). Consistent with our observations in cultured neurons [3], deleting *snapin* in embryonic mouse brain results in enhanced translocation of cytosolic LC3-I into membrane-bound and autophagic vacuole-enriched LC3-II. Intracellular protein quality control via the autophagy–lysosomal system is particularly important for maintaining cellular homoeostasis and cell survival [6]. Defects within this system ultimately lead to impaired neurodevelopment [12] and neurodegeneration [10,11]. The reduced cell density in *snapin*$^{-/-}$ embryonic mouse brains is probably due to impairment of the autophagy–lysosomal system.

Aberrant accumulation of polyubiquitinated proteins in *snapin*$^{-/-}$ embryonic mouse brain

In addition to the autophagy–lysosomal system, the ubiquitin–proteasome system accounts for a more selective intracellular protein degradation. Impairment of autophagy in the central nervous system is accompanied by the accumulation of ubiquitinated proteins [10–12]. Thus we explored whether the levels of polyubiquitinated proteins are altered in the *snapin*-deficient embryonic mouse brain. Immunoblots of brain homogenates show that the signal intensity of polyubiquitinated proteins is significantly increased in *snapin* homozygous mutant brains (Figures 4A and 4B); as a control there is no observable difference in the Golgi marker p115 among littermates of all three genotypes. Next, we examined ubiquitin expression in E18 mouse brains by co-immunostaining with antibodies against ubiquitin, a neuronal nuclear marker (NeuN) and nuclei (TO-PRO-3). Ubiquitin-positive aggregates and inclusion bodies were present in cells that were also positive for NeuN in *snapin*$^{-/-}$ embryonic cortex and hippocampus. In contrast, a few ubiquitin-positive puncta were detected in the *snapin* WT mouse brain under the same experimental conditions (Figures 4C and 4D). Both biochemical and immunohistochemical assays consistently suggest that defective autophagy–lysosomal pathways lead to the accumulation of polyubiquitinated proteins in the embryonic mouse brain, reflecting severe impairment of the cellular degradation and homoeostatic processes in the central nervous system. Thus our results indicate that Snapin has a central role in the clearance of unfavourable proteins and neuronal survival.

DISCUSSION

As the main synthetic and degradative compartments are located in the soma, the maintenance of neuronal function and survival is dependent upon efficient intracellular transport. Long-distance retrograde transport returns organelles to the soma and requires minus-end-directed dynein motors. Late endocytic membrane trafficking, which delivers internalized materials and newly synthesized hydrolases into lysosomes, is critical for maintaining efficient degradation capacities [1]. Autophagy is a critical homoeostatic process in which autophagosomes, containing bulk cytoplasmic components and organelles, fuse with lysosomes to form degradative autolysosomes [19–23]. Snapin acts as an adaptor that links late endosomes to dynein motors and therefore plays a key role in co-ordinating dynein-driven retrograde transport, late endosomal–lysosomal trafficking and lysosomal maturation [3]. The co-ordination of these processes in neurons is essential for the maintenance of efficient degradation capacity and cellular homoeostasis via the autophagy–

lysosomal pathway. The role of these dynamic cellular processes in the development of the central nervous system, however, remains to be evaluated.

It is well established that autophagy helps control cell proliferation and promote cell survival. Altered autophagy function has been linked to cell death [24,25], although the question of whether mammalian cell death can occur directly by autophagy or just programmed cell death accompanied by altered autophagy remains to be addressed [26]. The application of the autophagy–lysosomal fusion inhibitors bafilomycin A1 and chloroquine leads to the accumulation of LC3-II-labelled autophagic vesicles and cell apoptosis [27,28]. Between early embryonic stages and adulthood, more than half of the neurons in the developing nervous system are eliminated by programmed cell death under physiological and pathological conditions [29]. Impairment of the autophagy–lysosomal system has been implicated in the pathogenesis of a number of neurodegenerative diseases [6]. The autophagy-regulatory Atg family members are highly conserved throughout evolution from the yeast to eukaryotes. Deficiency in a principal regulator of autophagosome formation, Beclin 1 (Atg6), produces lethality at E7.5 due to failed visceral endoderm formation [7,30]. The Beclin-interacting protein Ambra-1 is exclusively expressed in vertebrates and regulates autophagy by forming a complex with Beclin and Vps34 (vacuolar protein sorting 34). *Ambra1* deletion severely inhibits the Beclin1-mediated induction of autophagy. Mouse embryos deficient in Ambra-1 die during embryonic stages and display defects in neural tube closure and cell death [12]. Thus cell survival, especially during nervous system development, depends upon the proper function of autophagy pathways.

In the present study, we focused on evaluating the role of Snapin-co-ordinated cellular processes in the development of the central nervous system using the *snapin*-deficient mouse embryonic brains. This study demonstrates that defective transport of late endosomes results in the following three major defects: (i) reduced cell density in cortical plates and intermediate zones; (ii) increased neuronal death in the cortex and third ventricular region; and (iii) the accumulation of LC3-II-labelled autophagic vacuoles and polyubiquitinated proteins in the cortex and hippocampus. Thus, the present study provides a new line of *in vivo* evidence that Snapin-mediated and dynein-driven retrograde transport of late endosomes is necessary for the maintenance of neuronal survival and development of the mammalian central nervous system.

The ubiquitin–proteasome and autophagy–lysosome pathways are the main cellular processes responsible for the clearance of misfolded and/or aggregated proteins and dysfunctional organelles in eukaryotic cells (see the review [31]). Dysfunction of these pathways contributes to the pathology of various neurodegenerative conditions (see the review [5]). Polyglutamine-expansion mutations, mutant forms of α-synuclein and different forms of tau protein are cleared mainly by the autophagy–lysosomal pathway [32–38]. Targeted mutation of essential and regulatory autophagy genes leads to the formation of polyubiquitinated aggregates and excessive apoptotic cell death in mouse brains [8,11,12]. In our *snapin*$^{-/-}$ mouse embryonic brains, we consistently observed impaired turnover of autolysosomes and increased accumulation of polyubiquitinated aggregates, both indicative of defects in degradative processes. Thus Snapin-mediated late endocytic transport is essential for protein quality control and neuronal survival.

It is also possible that Snapin-mediated and dynein-driven retrograde transport delivers survival signals, such as neurotrophin–Trk (tropomyosin receptor kinase) complexes packaged in 'signalling endosomes', to the soma [39–41]. *Snapin* deficiency may impact neuronal survival more prominently during the early development stage. It will be interesting to examine the transport properties of these 'signalling endosomes' in the *snapin*$^{-/-}$ mouse model in future studies. In addition, the *snapin*-KO mouse represents one of the few genetic models with such striking phenotypes and will serve as a unique genetic tool for characterizing the role of late endocytic transport in the clearance of aggregated protein and dysfunctional organelles during neurodevelopment and neurodegeneration.

Acknowledgments

We thank members of Z.-H.S.'s laboratory for helpful discussions, and M. Davis for editing the manuscript prior to submission. B.Z. and Y.-B.Z. are graduate students of the NIH–Shanghai JiaoTong University Joint Ph.D. Program in Neuroscience.

FUNDING

This work was supported by the Intramural Research Program of the National Institute of Neurological Disorders and Stroke, National Institutes of Health (to Z.-H.S.).

Abbreviations used

E18 etc.	embryonic day 18 etc.
KO	knockout
NeuN	neuronal nuclei
TUNEL	terminal deoxynucleotidyl transferase-mediated dUTP nick-end labelling
WT	wild-type

REFERENCES

1. Luzio JP, Pryor PR, Bright NA. Lysosomes: fusion and function. Nat. Rev. Mol. Cell. Biol. 2007; 8:622–632. [PubMed: 17637737]
2. Overly CC, Hollenbeck PJ. Dynamic organization of endocytic pathways in axons of cultured sympathetic neurons. J. Neurosci. 1996; 16:6056–6064. [PubMed: 8815888]
3. Cai Q, Lu L, Tian J-H, Zhu Y-B, Qiao H, Sheng Z-H. Snapin-regulated late endosomal transport is critical for efficient autophagy–lysosomal function in neurons. Neuron. 2010; 68:73–86. [PubMed: 20920792]
4. Lee JH, Yu WH, Kumar A, Lee S, Mohan PS, Peterhoff CM, Wolfe DM, Martinez-Vicente M, Massey AC, Sovak G, et al. Lysosomal proteolysis and autophagy require presenilin 1 and are disrupted by Alzheimer-related PS1 mutations. Cell. 2010; 141:1146–158. [PubMed: 20541250]
5. Rubinsztein DC. The roles of intracellular protein-degradation pathways in neurodegeneration. Nature. 2006; 443:780–786. [PubMed: 17051204]
6. Levine B, Kroemer G. Autophagy in the pathogenesis of disease. Cell. 2008; 132:27–42. [PubMed: 18191218]
7. Yue Z, Jin S, Yang C, Levine AJ, Heintz N. Beclin 1, an autophagy gene essential for early embryonic development, is a haploinsufficient tumor suppressor. Proc. Natl. Acad. Sci. U.S.A. 2003; 100:15077–15082. [PubMed: 14657337]

8. Komatsu M, Waguri S, Ueno T, Iwata J, Murata S, Tanida I, Ezaki J, Mizushima N, Ohsumi Y, Uchiyama Y, et al. Impairment of starvation-induced and constitutive autophagy in Atg7-deficient mice. J. Cell Biol. 2005; 169:425–434. [PubMed: 15866887]
9. Kuma A, Hatano M, Matsui M, Yamamoto A, Nakaya H, Yoshimori T, Ohsumi Y, Tokuhisa T, Mizushima N. The role of autophagy during the early neonatal starvation period. Nature. 2004; 432:1032–1036. [PubMed: 15525940]
10. Hara T, Nakamura K, Matsui M, Yamamoto A, Nakahara Y, Suzuki-Migishima R, Yokoyama M, Mishima K, Saito I, Okano H, Mizushima N. Suppression of basal autophagy in neural cells causes neurodegenerative disease in mice. Nature. 2006; 441:885–889. [PubMed: 16625204]
11. Komatsu M, Waguri S, Chiba T, Murata S, Iwata J, Tanida I, Ueno T, Koike M, Uchiyama Y, Kominami E, Tanaka K. Loss of autophagy in the central nervous system causes neurodegeneration in mice. Nature. 2006; 441:880–884. [PubMed: 16625205]
12. Fimia GM, Stoykova A, Romagnoli A, Giunta L, Di Bartolomeo S, Nardacci R, Corazzari M, Fuoco C, Ucar A, Schwartz P, et al. Ambra1 regulates autophagy and development of the nervous system. Nature. 2007; 447:1121–1125. [PubMed: 17589504]
13. Tian JH, Wu ZX, Unzicker M, Lu L, Cai Q, Li C, Schirra C, Matti U, Stevens D, Deng C, et al. The role of Snapin in neurosecretion: snapin knock-out mice exhibit impaired calcium-dependent exocytosis of large dense-core vesicles in chromaffin cells. J. Neurosci. 2005; 25:10546–10555. [PubMed: 16280592]
14. Pan PY, Tian JH, Sheng ZH. Snapin facilitates the synchronization of synaptic vesicle fusion. Neuron. 2009; 61:412–424. [PubMed: 19217378]
15. Buxton P, Zhang XM, Walsh B, Sriratana A, Schenberg I, Manickam E, Rowe T. Identification and characterization of Snapin as a ubiquitously expressed SNARE-binding protein that interacts with SNAP23 in non-neuronal cells. Biochem. J. 2003; 375:433–440. [PubMed: 12877659]
16. Starcevic M, Dell'Angelica EC. Identification of snapin and three novel proteins (BLOS1, BLOS2, and BLOS3/reduced pigmentation) as subunits of biogenesis of lysosome-related organelles complex-1 (BLOC-1). J. Biol. Chem. 2004; 279:28393–28401. [PubMed: 15102850]
17. Lu L, Cai Q, Tian JH, Sheng ZH. Snapin associates with late endocytic compartments and interacts with late endosomal SNAREs. Biosci. Rep. 2009; 29:261–269. [PubMed: 19335339]
18. Kabeya Y, Mizushima N, Ueno T, Yamamoto A, Kirisako T, Noda T, Kominami E, Ohsumi Y, Yoshimori T. LC3, a mammalian homologue of yeast Apg8p, is localized in autophagosome membranes after processing. EMBO J. 2000; 19:5720–5728. [PubMed: 11060023]
19. Dunn WA Jr. Autophagy and related mechanisms of lysosome-mediated protein degradation. Trends Cell Biol. 1994; 4:139–143. [PubMed: 14731737]
20. Klionsky DJ, Emr SD. Autophagy as a regulated pathway of cellular degradation. Science. 2000; 290:1717–1721. [PubMed: 11099404]
21. Mizushima N, Ohsumi Y, Yoshimori T. Autophagosome formation in mammalian cells. Cell Struct. Funct. 2002; 27:421–429. [PubMed: 12576635]
22. Levine B, Klionsky DJ. Development by self-digestion: molecular mechanisms and biological functions of autophagy. Dev. Cell. 2004; 6:463–477. [PubMed: 15068787]
23. Levine B, Yuan J. Autophagy in cell death: an innocent convict? J. Clin. Invest. 2005; 115:2679–2688. [PubMed: 16200202]
24. Kroemer G, Jaattela M. Lysosomes and autophagy in cell death control. Nat. Rev. Cancer. 2005; 5:886–897. [PubMed: 16239905]
25. Cecconi F, Levine B. The role of autophagy in mammalian development: cell makeover rather than cell death. Dev. Cell. 2008; 15:344–357. [PubMed: 18804433]
26. Levine B, Kroemer G. Autophagy in aging, disease and death: the true identity of a cell death impostor. Cell Death Differ. 2009; 16:1–2. [PubMed: 19079285]
27. Yamamoto A, Tagawa Y, Yoshimori T, Moriyama Y, Masaki R, Tashiro Y. Bafilomycin A1 prevents maturation of autophagic vacuoles by inhibiting fusion between autophagosomes and lysosomes in rat hepatoma cell line, H-4-II-E cells. Cell Struct. Funct. 1998; 23:33–42. [PubMed: 9639028]

28. Boya P, Gonzalez-Polo RA, Casares N, Perfettini JL, Dessen P, Larochette N, Metivier D, Meley D, Souquere S, Yoshimori T, et al. Inhibition of macroautophagy triggers apoptosis. Mol. Cell. Biol. 2005; 25:1025–1040. [PubMed: 15657430]
29. Xie Z, Klionsky DJ. Autophagosome formation: core machinery and adaptations. Nat. Cell Biol. 2007; 9:1102–1109. [PubMed: 17909521]
30. Liang XH, Jackson S, Seaman M, Brown K, Kempkes B, Hibshoosh H, Levine B. Induction of autophagy and inhibition of tumorigenesis by beclin 1. Nature. 1999; 402:672–676. [PubMed: 10604474]
31. Tai HC, Schuman EM. Ubiquitin, the proteasome and protein degradation in neuronal function and dysfunction. Nat. Rev. Neurosci. 2008; 9:826–838. [PubMed: 18931696]
32. Ravikumar B, Vacher C, Berger Z, Davies JE, Luo S, Oroz LG, Scaravilli F, Easton DF, Duden R, O'Kane CJ, Rubinsztein DC. Inhibition of mTOR induces autophagy and reduces toxicity of polyglutamine expansions in fly and mouse models of Huntington disease. Nat. Genet. 2004; 36:585–595. [PubMed: 15146184]
33. Wong E, Cuervo AM. Autophagy gone awry in neurodegenerative diseases. Nat. Neurosci. 13:805–811. [PubMed: 20581817]
34. Webb JL, Ravikumar B, Atkins J, Skepper JN, Rubinsztein DC. α-Synuclein is degraded by both autophagy and the proteasome. J. Biol. Chem. 2003; 278:25009–25013. [PubMed: 12719433]
35. Qin ZH, Wang Y, Kegel KB, Kazantsev A, Apostol BL, Thompson LM, Yoder J, Aronin N, DiFiglia M. Autophagy regulates the processing of amino terminal huntingtin fragments. Hum. Mol. Genet. 2003; 12:3231–3244. [PubMed: 14570716]
36. Iwata A, Riley BE, Johnston JA, Kopito RR. HDAC6 and microtubules are required for autophagic degradation of aggregated huntingtin. J. Biol. Chem. 2005; 280:40282–40292. [PubMed: 16192271]
37. Berger Z, Ravikumar B, Menzies FM, Oroz LG, Underwood BR, Pangalos MN, Schmitt I, Wullner U, Evert BO, O'Kane CJ, Rubinsztein DC. Rapamycin alleviates toxicity of different aggregate-prone proteins. Hum. Mol. Genet. 2006; 15:433–442. [PubMed: 16368705]
38. Shibata M, Lu T, Furuya T, Degterev A, Mizushima N, Yoshimori T, MacDonald M, Yankner B, Yuan J. Regulation of intracellular accumulation of mutant Huntingtin by Beclin 1. J. Biol. Chem. 2006; 281:14474–14485. [PubMed: 16522639]
39. Deinhardt K, Salinas S, Verastegui C, Watson R, Worth D, Hanrahan S, Bucci C, Schiavo G. Rab5 and Rab7 control endocytic sorting along the axonal retrograde transport pathway. Neuron. 2006; 52:293–305. [PubMed: 17046692]
40. Perlson E, Jeong GB, Ross JL, Dixit R, Wallace KE, Kalb RG, Holzbaur EL. A switch in retrograde signaling from survival to stress in rapid-onset neurodegeneration. J. Neurosci. 2009; 29:9903–9917. [PubMed: 19657041]
41. Cosker KE, Courchesne SL, Segal RA. Action in the axon: generation and transport of signaling endosomes. Curr. Opin. Neurobiol. 2008; 18:270–275. [PubMed: 18778772]

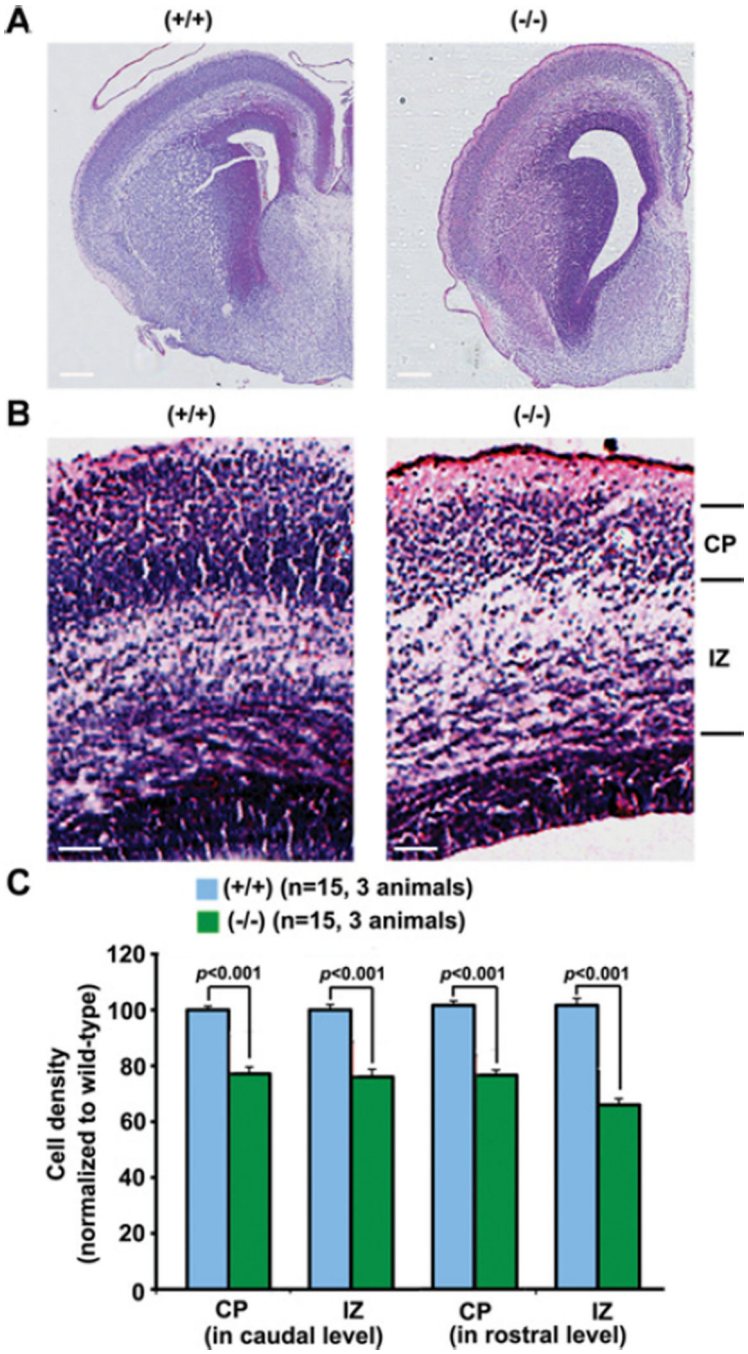

Figure 1. Reduced cell density in cortical plates and intermediate zones of *snapin*$^{-/-}$ embryonic mouse brains

(A) Brains from E18 *snapin*$^{+/+}$ and *snapin*$^{-/-}$ embryos were stained with haematoxylin and eosin. (B) High-magnification images from representative brain slices. Note that at E18, cell densities in both cortical plates (CP) and intermediate zones (IZ), marked on the right, are significantly decreased in *snapin*$^{-/-}$ mice compared with their *snapin*$^{+/+}$ littermates. (C) Quantification of cell densities in both CP and IZ regions. Data were normalized against values from *snapin*$^{+/+}$ littermates. Cell densities are significantly decreased ($P < 0.001$) in caudal and rostral levels of the *snapin*$^{-/-}$ brains. A two-tailed Student's *t* test for paired data

was used and error bars indicate S.E.M. A total of 15 brain slices from three pairs of littermates were examined. Scale bars: (A) 200 μm and (B) 10 μm.

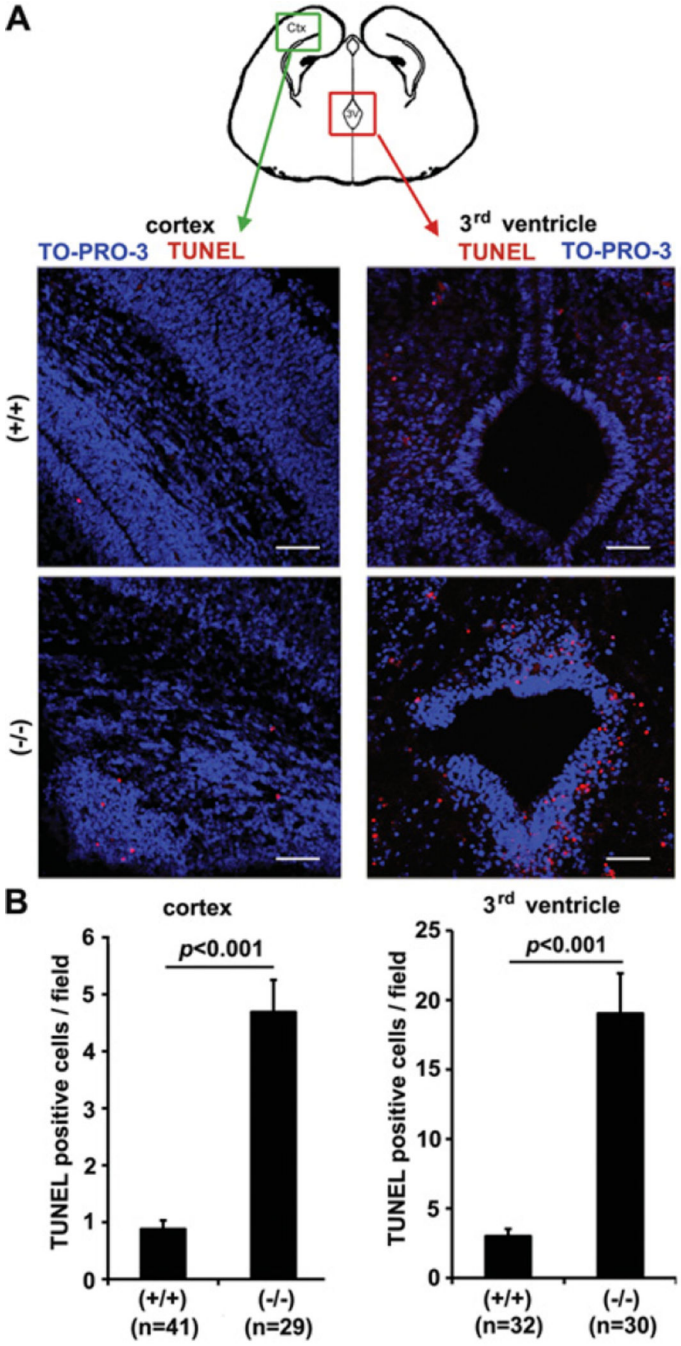

Figure 2. Increased apoptotic cell death in the cortex and third ventricle of E18 *snapin*$^{-/-}$ mice

(A) Representative images showing increased TUNEL-positive cells in the cortex and third ventricle. Coronal sections of the cortex and third ventricle were co-stained with TUNEL (red), a marker for apoptosis, and TO-PRO-3 (blue), a nuclear marker. The top panel is a schematic diagram showing the location of the cortex and third ventricle in developing mouse brain. Scale bars: 50 μm. (B) Average number of TUNEL-positive cells per imaging field at ×40 magnification within the cortex (left) and third ventricular region (right) of *snapin*$^{-/-}$ and *snapin*$^{+/+}$ embryos. Images were obtained from three pairs of littermates, and

the total number of slice images used for each genotype is included in parentheses. Data are expressed as means ± S.E.M.

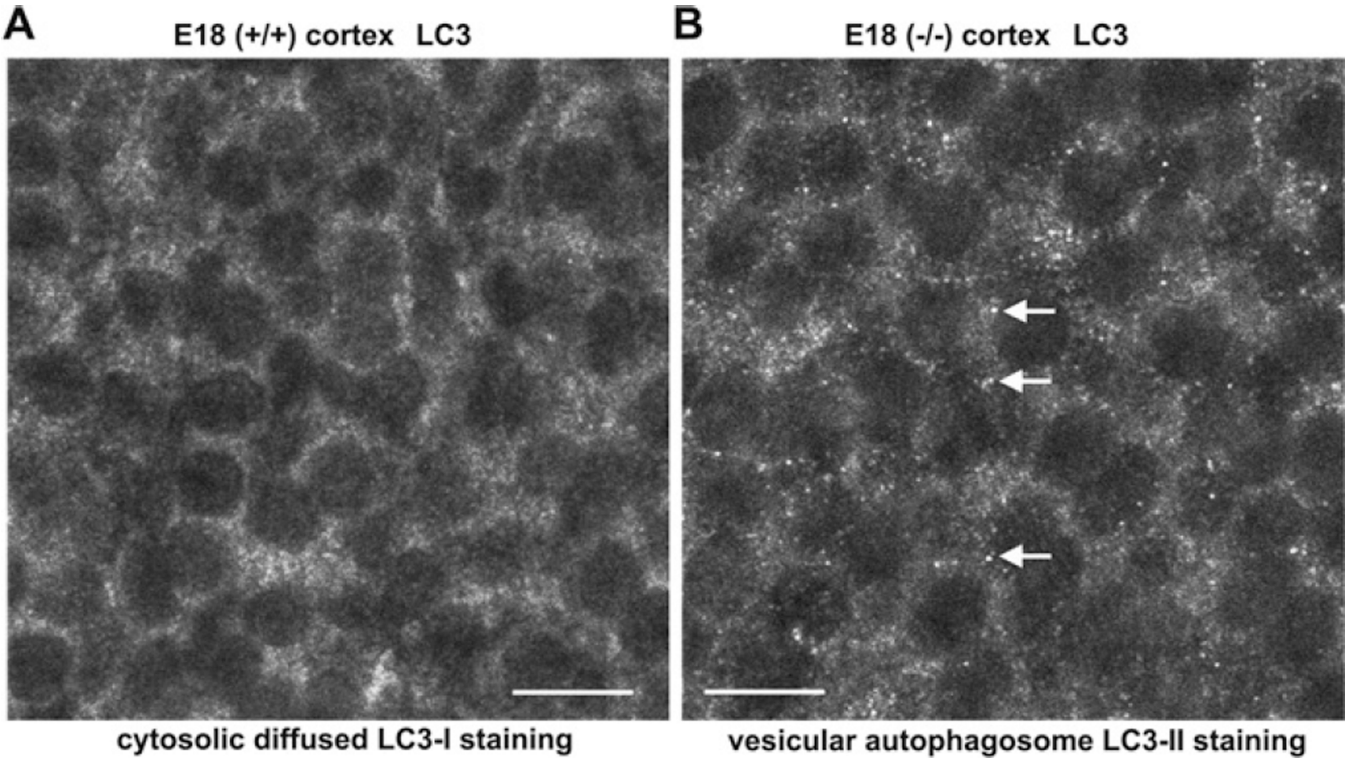

Figure 3. Increased LC3-II-labelled vesicular autophagosome in *snapin*$^{-/-}$ embryonic cortex

Representative images showing LC3 distribution in layer II/III of E18 cortex. Coronal sections of the cortex were stained with anti-LC3 antibody. Note that LC3 staining was primarily cytosolic and diffuse in *snapin*$^{+/+}$ cortex (A), whereas *snapin*$^{-/-}$ mice display a punctate pattern (B). Deleting snapin results in enhanced translocation of cytosolic LC3-I into membrane-bound and autophagic vacuole-enriched LC3-II (indicated by arrows). Scale bars, 10 μm.

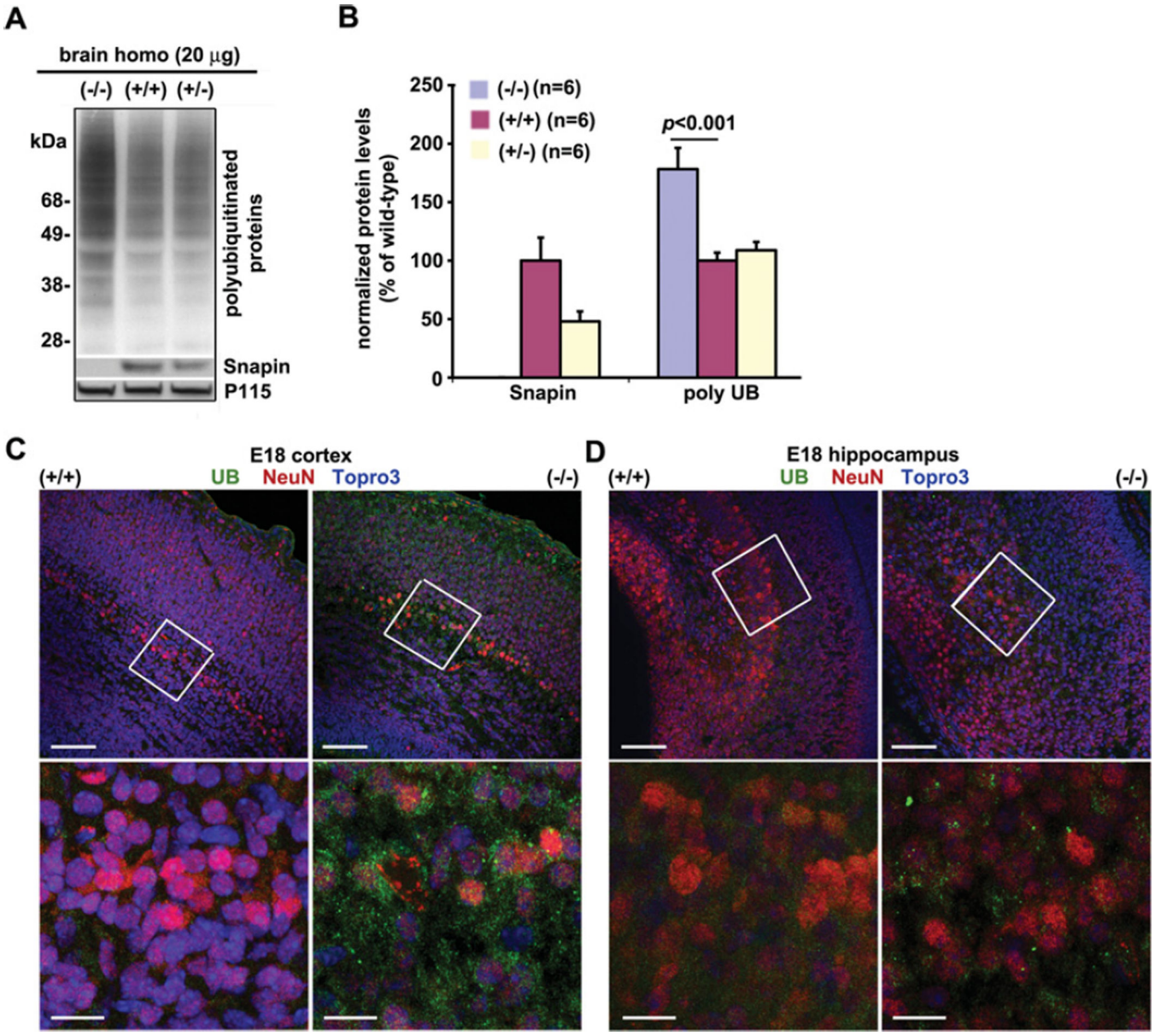

Figure 4. Accumulation of polyubiquitinated proteins in *snapin*$^{-/-}$ embryonic mouse brain

(A) Representative immunoblot showing increased ubiquitinated proteins in E18 *snapin*$^{-/-}$ mouse brain relative to its *snapin*$^{+/+}$ and *snapin*$^{+/-}$ littermates. Brain homogenates (homo) (20 μg) were resolved by SDS/PAGE and sequentially probed with antibodies on the same membranes after stripping between the applications of each antibody. The Golgi marker p115 served as a loading control. (B) Quantification of normalized Snapin and polyubiquitin (poly UB) protein levels in the brains (E18) of three *snapin* genotypes. The protein intensity of polyubiquitin and Snapin (gels = 6) was normalized against p115 and is displayed as a percentage ratio relative to *snapin*$^{+/+}$ control. A two-tailed Student's *t* test for paired data was used and error bars indicate S.E.M. (C, D) Representative images showing increased ubiquitin-positive cells in brains of *snapin*$^{-/-}$ embryos. Coronal sections of the brain cortex (C) and hippocampus (D) from E18 embryos were stained with antibodies against ubiquitin

(UB; green), NeuN (neuron-specific nuclear protein; red) and nuclei (TO-PRO-3; blue). The lower panels are high-magnification images of the boxed regions of the upper panels. Note that ubiquitin puncta accumulate in *snapin*$^{-/-}$ cortex and hippocampus. Scale bars: 20 μm in low magnification and 50 μm in high magnification.